

# THE FATE OF OIL CLUSTERS DURING FRACTIONAL FLOW: TRAJECTORIES IN THE SATURATION-CAPILLARY NUMBER SPACE

M. Rücker<sup>2,1</sup>, S. Berg<sup>1</sup>, R. Armstrong<sup>3,1</sup>, A. Georgiadis<sup>1,5</sup>, H. Ott<sup>1,6</sup>, L. Simon<sup>2</sup>, F. Enzmann<sup>2</sup>, M. Kersten<sup>2</sup>, S. de With<sup>4,1</sup>

<sup>1</sup>Shell Global Solutions International, Kesslerpark 1, 2288 GS Rijswijk, Netherlands

<sup>2</sup>Geosciences Institute, Johannes-Gutenberg University, 55099 Mainz, Germany

<sup>3</sup>School of Petroleum Engineering, University of New South Wales, New South Wales, Sydney, Australia

<sup>4</sup>Technical University Delft, Stevinweg 1, 2628 CN Delft, Netherlands

<sup>5</sup>also at: Department of Chemical Engineering, Imperial College London, SW7 2AZ UK

<sup>6</sup>also at: Department of Earth Science and Engineering, Imperial College London, SW7 2AZ UK

*This paper was prepared for presentation at the International Symposium of the Society of Core Analysts held in St. John's Newfoundland and Labrador, Canada, 16-21 August, 2015*

## ABSTRACT

Fractional flow has been studied at the pore scale under dynamic flow conditions by using fast synchrotron-based X-ray computed micro-tomography. The pore-scale flow regimes have been mapped in a “phase diagram” where the regimes of connected pathway flow and ganglion dynamics are characterized by fractional flow and capillary number. The regimes are identified from the respective pore scale dynamics that can be conveniently characterized by using a saturation-(cluster-based) capillary number diagram. Therein connected pathway flow is represented by a fixed point (because all parameters are constant over time) and in ganglion dynamic regime the oil clusters follow trajectories because saturation and cluster length are changing over time. Ganglion dynamics is composed of breakup and coalescence processes. During coalescence processes, both cluster volume and length increases, i.e. clusters move “up” the trajectory. During break-up processes, on the other hand, both properties decrease and clusters move “down” the trajectory.

Ganglion dynamics occurred even though the (cluster-based) capillary number of the average flow field was at least two orders of magnitude smaller than unity, i.e. the average flow field indicates capillary-dominated regime. However viscous mobilization can also be triggered by more complex break-up and coalescence processes that have much higher local flow velocities than the average flow field suggests. Most situations encountered are a combination of connected pathway flow and ganglion dynamics, where a combination of viscous and capillary-driven processes accounts for the net transport of oil. Static simulation approaches are not capable of capturing such regimes, as they require connected pathway flow.

## INTRODUCTION

During the recovery of oil from an underground reservoir by water flooding, the non-wetting oil phase is displaced by the wetting water phase. Corresponding to the Buckley–Leverett equation [1], the two fluids flow simultaneously through narrow pore space once the saturation front has passed. In order to determine the relative permeability of this simultaneous flow, commonly steady-state core flooding experiments (e.g., experiments on 5cm-long rock samples) are conducted [2]. However, core flood experiments often show fluctuations of parameters such as saturation, pressure and resistivity depending on the fractional flow (Figure 1). The reason for these fluctuations is not fully clear yet, but may be related to different flow regimes [3, 4, 5].

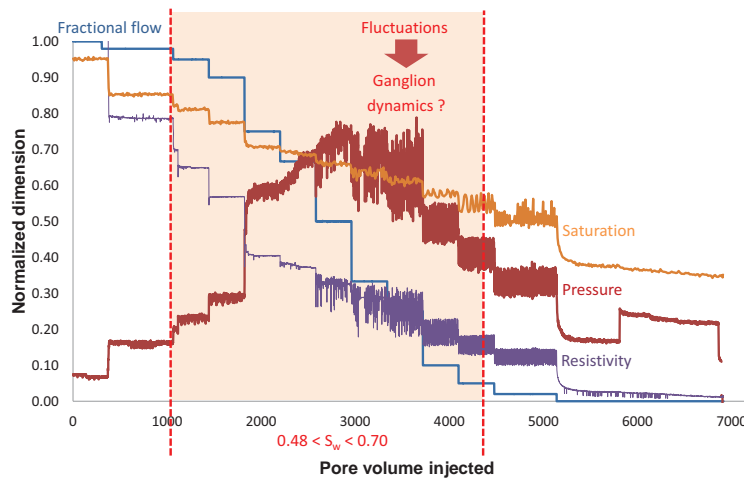


**Figure 1** Results of a core flood experiment measured on a 5 cm rock sample (right) show a variation of fluctuations in different parameters such as saturation, pressure, and resistivity depending on the fractional flow (left).

On the pore scale, Avraam and Payatakes [3] observed three types of flow regime, which are (i) connected pathway flow, (ii) drop traffic flow, and (iii) ganglion dynamics. During connected pathway flow, the non-wetting and the wetting phases move mainly through their respective connected networks [3]. The drop traffic regime describes the flow of oil through disconnected droplets smaller than the diameter of the pore throats [3]. These are formed by vigorous break-up of the oil ganglia and are stabilized by the flow of the surrounding water, which prevents the growing of ganglia via coalescence [3]. The most complex flow regime is the ganglion dynamics, whereby oil is disconnected into ganglia with sizes larger than a pore. These ganglia move or get immobilized in narrow passages, they break into smaller ganglia and get trapped even more easily, or they collide with other ganglia, grow and get remobilized [3]. The thus prevailing flow regime depends on different parameters such as viscosity, wettability, surface tension, flow rate ratio, capillary number, etc. [4]. For specific fluids in a specific porous medium most parameters are constant and the relative permeability appears to be a function of capillary number and flow rate ratio [8].

While most previous studies performed on dynamic two-phase flow are either based on 2D models [3,9] or on 3D but indirectly measured [4, 5] or on simulations [6, 7], in this study we image directly the 3D development of clusters in real time by fast synchrotron based X-ray  $\mu$ CT. Recent studies using this technique allowed the first insights into pore-scale processes during drainage and imbibition [10, 11, 12, 13] such as Haines jumps [14, 15, 16], coalescence [17,18] and snap-off [18, 19]. In this study we analysed ganglion dynamics by co-injection of two fluids at different ratios and velocities in porous media in order to determine the prevailing flow regime.

## MATERIALS AND METHODS

For this experiment, n-decane was used as nonwetting phase and brine as wetting phase. A strongly water-wet sintered glass sample (4 mm diameter, 20 mm length, embedded into a polycarbonate tube by heat-shrinking) with a porosity of 35% and permeability of  $22 \pm 2$  D was mounted at the top of a flow cell. The flow cell was specially designed for fractional flow experiments and contained two remotely controlled micro piston pumps, which enables continuous rotation of the sample and constant data acquisition in the field of view during the experiment. A full 3D image with a voxel size of  $2.2 \mu\text{m}$  was obtained in 1 min. The measurements were performed at a fast synchrotron-based X-ray computed microtomography facility (TOMCAT beamline, Swiss Light Source, Paul Scherrer Institute). Details on the flow cell and the experimental settings were described previously [20]. The reconstructed  $\mu$ CT images were filtered, segmented and processed with the software package AVIZO 8 (Visualization Science group).

Subsequently, the resulting binarized images containing the porous medium and the oil and water phases were used for further analyses, e.g., for estimation of the relative permeability. The single-phase flow simulation by the software package GeoDICT (Math2Market) was used in the Navier-Stokes mode to calculate the permeability through the connected portion of the oil- and water-phase for each time step.

Furthermore, all flow events occurring during the experiment were determined and separated into oil-filling and water-filling events. While the former event type describes a situation in which pores drained from water are filled by oil, the latter type corresponds to oil being replaced by water. The events are determined by generating a differential image of two consecutive 3D binary images containing only the oil phase. The differential image gives the position and size of both water- or oil-filling events. A single event is defined as a spatially separated fluid change at a specific position. The event size is defined as the volume of the spatially separated change. To reduce effects due to noise, small events ( $< (21 \mu\text{m})^3$  corresponding to 10 voxels in each direction) are ignored.

In addition, the development of clusters was observed. To follow a chosen cluster through the different time steps, the space occupied by this cluster in the first time step is compared to the same space in the next time step. All clusters inside this space or connected to this space are then used as a mask for the next time step. This procedure is

iterated over all measured time steps, enabling clusters to be tracked over time and statistics to be obtained.

## RESULTS AND DISCUSSION

The flow regime depends on the fractional flow and the capillary number. The fractional flow is given by the injection rate ratio of each fluid to the total fluid, while the capillary number in this study is determined by the macroscopic cluster-based definition [9, 24]:

$$Ca^{macro} = \frac{l^{cl}}{r_p} \varphi \frac{\mu_w v_w}{\gamma_{w,nw}}, \quad (1)$$

With the cluster length ( $l^{cl}$ ), radius of a pore throat ( $r_p$ ), porosity ( $\varphi$ ), viscosity of the wetting phase ( $\mu_w$ ), interstitial velocity of the wetting phase ( $v_w$ ), and interfacial tension ( $\gamma_{w,nw}$ ). The radius of the peak pore size of the pore size distribution calculated by the software code GeoDICT was used as pore throat radius. The velocity is derived from the injection rate and represents the average flow field, which is often used to characterize a flow regime. An overall  $\overline{Ca}^{macro}$  was calculated by averaging  $l^{cl}$  of all clusters as described in [24]. The fractional flow-capillary number diagram (Figure 2) shows how the experiments were conducted, starting at a high water fraction and low total injection rate of  $4 \times 10^{-6}$  m/s corresponding to a low  $\overline{Ca}^{macro}$ . The total injection rate increased stepwise up to  $4 \times 10^{-4}$  m/s before changing to a lower oil fraction. For all experiments  $\overline{Ca}^{macro} < 1$  indicating capillary dominated flow regime. However, since local velocities may deviate from the overall velocity, the transition from capillary dominated to viscous dominated regimes is rather smooth.

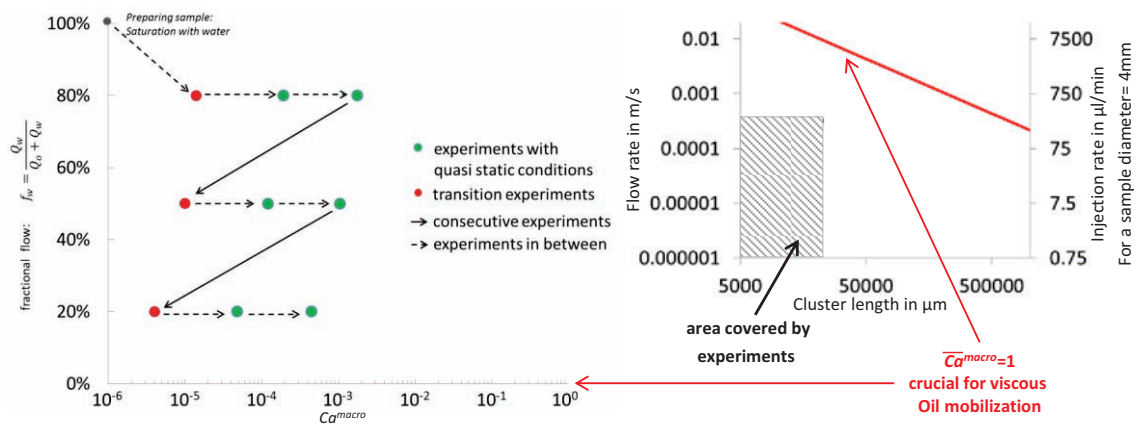


**Figure 2** The experiments started with a high water fraction (80% water) and a low flow rate ( $4 \times 10^{-6}$  m/s). The total injection rate was increased stepwise up to  $4 \times 10^{-4}$  m/s before repeating the experiments at a lower oil fraction (left). In all experiments, a  $\overline{Ca}^{macro} < 1$  corresponding to a capillary-dominated system (right).

In our experiments, we captured the transient regime when changing flow rates followed by the quasi steady-state regime. This transition could be recognized by the initial change in saturation. At low flow rates, the transition took longer and, therefore, was ideal for

observing growing and decreasing clusters. An increase in oil-saturation with a high frequency of oil-filling events appeared as Haines jumps and coalescence, while a decrease in saturation was dominated by snap-offs and led to disconnected clusters. For this reason, initial drainage led to a high connectivity, while in general a low saturation corresponded to low connectivity.

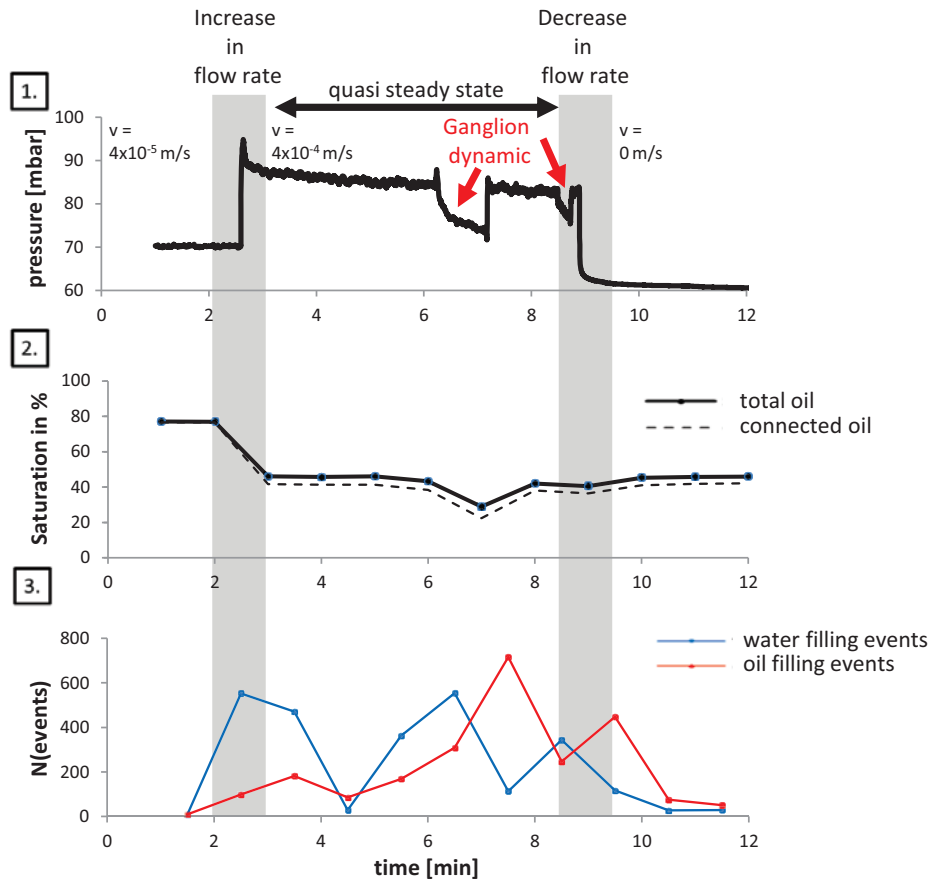


**Figure 3** Pressure (1), saturation (2), and event statistics (3) for an experiment at  $f_w = 0.5$  and a total flow rate of  $4 \times 10^{-4}$  m/s. Transitions between different fractional flows / flow rates where the target conditions had not been fully reached are marked by the grey bars. In these transition regimes, we observed natural changes in pressure, saturation, and pore-filling events, because flow conditions have been changed externally. However, in the quasi steady-state regime there are also pressure data and saturation fluctuations, which coincide with pore-scale water- and oil-filling events as signature of ganglion dynamics behavior.

The term “quasi” steady-state is chosen to indicate that fluctuations and events may still occur even though the average saturation has adjusted to the new injection rate. These fluctuations may be indicative of ganglion dynamics. At quasi steady-state conditions the saturation remained mostly stable and the number of events was smaller. Nevertheless, some fluctuations could be observed at water fraction  $f_w = 0.5$  and high total flow rates ( $4 \times 10^{-4}$  m/s, Figure 3). A sudden pressure drop followed by an increase occurred between the sixth and eighth minute (Figure 3.1). In the same time period, the oil volume dropped (Figure 3.2) and the number of water- and oil-filling events increased (Figure 3.3).

This observation is very similar in terms of saturation and pressure fluctuation to the results of core flood experiments at  $f_w = 0.5$  and 5 cm long rock samples.

### Growing and Shrinking Clusters

We tracked individual clusters to gain further insights into ganglion dynamics. In Figure 4, the development of a cluster that grows over time is shown.

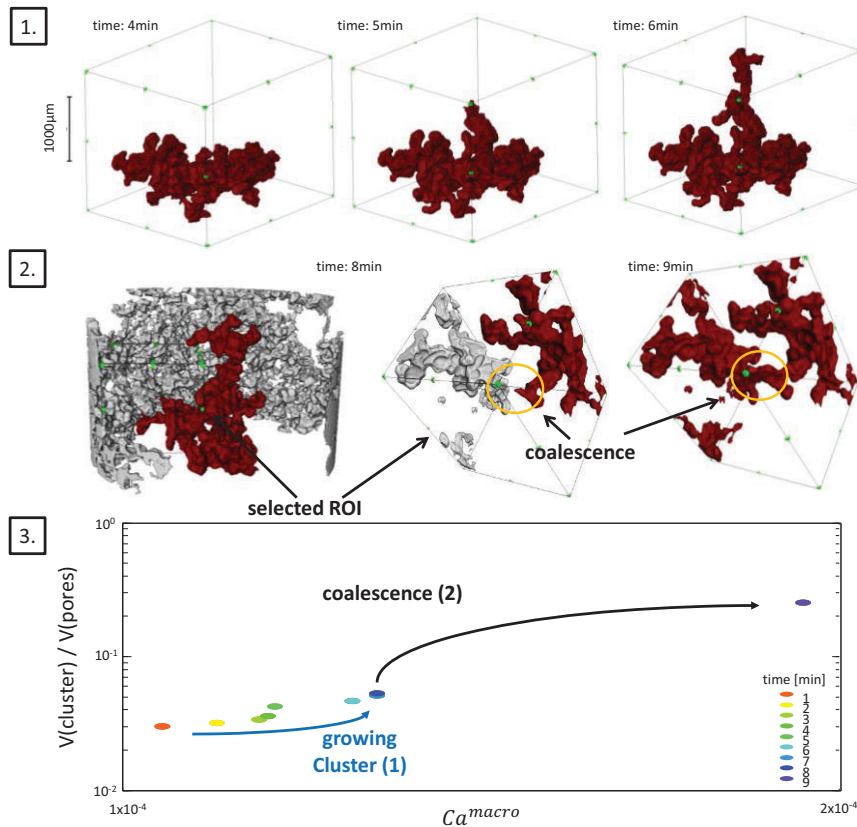


**Figure 4** Tracking a growing cluster at  $f_w = 0.8$  and  $v = 4 \times 10^6$  m/s: In the first phase (1), the cluster continuously increases in volume. For this reason, the corresponding cluster-trajectory in the cluster volume-capillary number ( $V-Ca$ ) space moves slowly towards high volume and capillary number, before it suddenly jumps (3) due to a coalescence with another cluster (2).

The cluster grows first through pathways outside the field of view by invading adjacent pores (Figure 4.1) before it coalesces with another cluster (Figure 4.2). In the volume- $Ca^{macro}$  space, this development is visible in a trajectory moving from low  $V-Ca^{macro}$  to high  $V-Ca^{macro}$  regime.

A “shrinking” cluster behaves differently, because in addition to a decrease in volume due to water film swelling [11] (and oil moving out the field of view), we also observe fragmentation. As shown in Figure 5, the cluster first decreases until snap-off events lead to fragmentation. The evolution of the saturation distribution of a shrinking cluster is

shown in Figure 5.1. The initial cluster A snaps off apart into two smaller clusters A and B. After redistribution of oil the volume apparently further decreases which is an imaging artifact from moving oil due to snap-off (few milliseconds [22]) during the acquisition time of a tomogram (60 s). Then cluster B snaps off into B and C. The corresponding trajectory in the  $V-Ca^{macro}$  space is in this case moving, vice versa, towards low volume and  $Ca^{macro}$ .

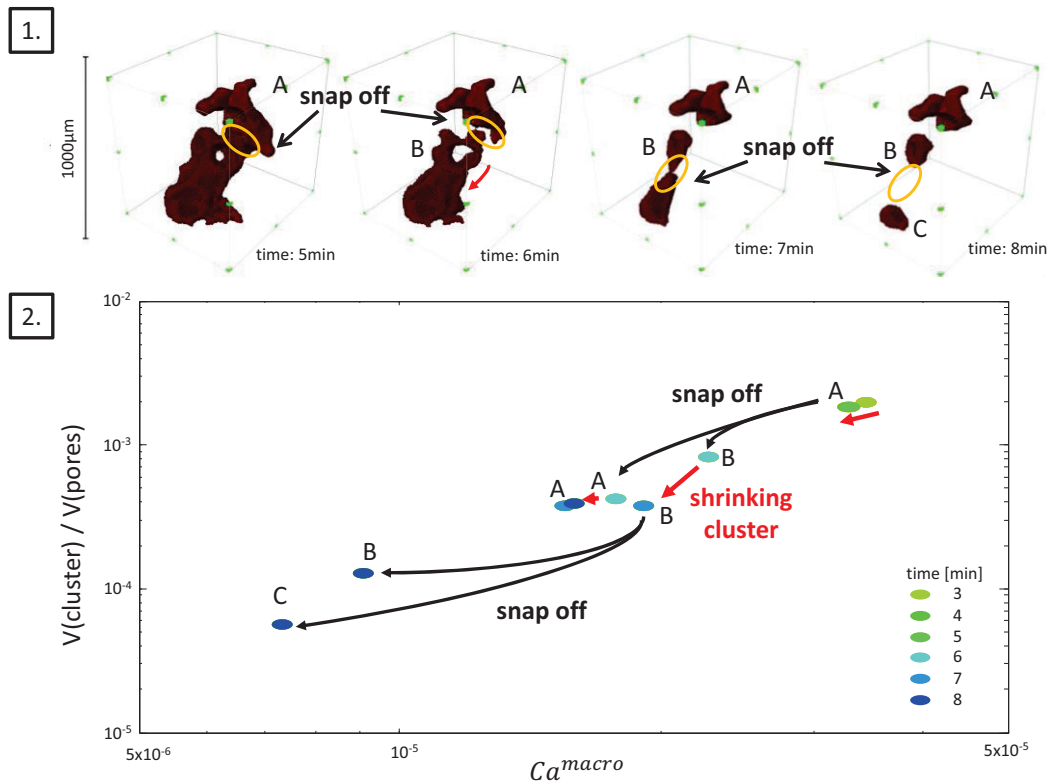


**Figure 5** Tracking a decreasing cluster at  $f_w = 0.5$  and high  $Ca$ . First, the cluster slowly decreases due to film swelling, before snap-off events fragment it into smaller ones, which further decrease in size and break apart. The clusters shown in (1.) correspond to the clusters shown in the trajectory (2.), where the single new appearing fragments are named A-C to indicate which fragment in later time steps is represented by which point in the diagram.

The cluster trajectories in the  $V-Ca^{macro}$  space move upwards when they are growing by coalescence or Haines jumps, and downwards while they snap off during shrinkage. However, all clusters have to be taken into account in order to determine the flow regime.

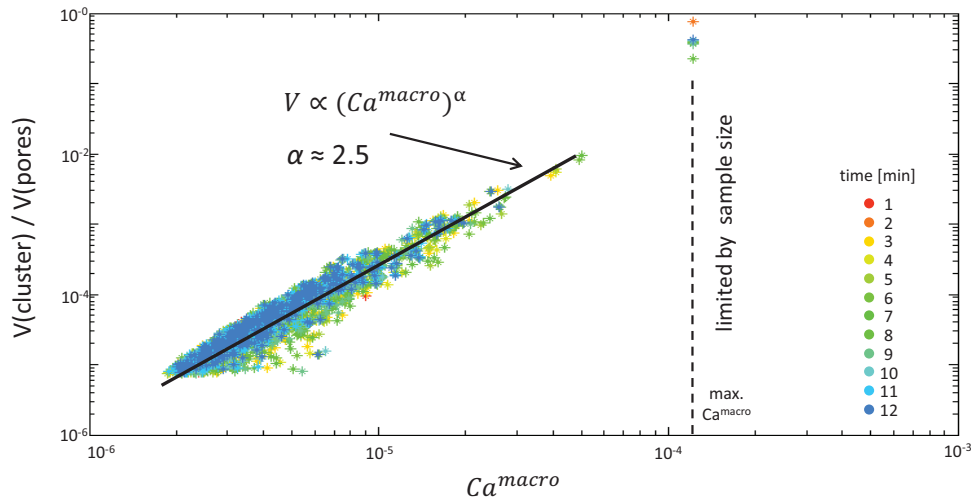


**Figure 6** All clusters for each time step at  $f_w = 0.5$  and  $v = 4 \times 10^{-4}$  m/s follow a power-law distribution with an exponent  $\alpha \approx 2.5$ , which gives information about the shape of the clusters. The capillary number of the largest clusters is limited by the sample size leading to a bias.

Figure 6 shows the distribution of all clusters for all time steps at  $f_w = 0.5$  and  $v = 4 \times 10^{-4}$  m/s. The distribution of the clusters appears to follow a power-law like behavior,  $V(\text{cluster}) \propto (Ca^{\text{macro}})^\alpha$ , with an average exponent  $\alpha \approx 2.5$ . Since  $Ca^{\text{macro}} \propto l^{cl}$ , the exponent gives information regarding the shape of the cluster. The exponent of  $\alpha = 2.5$  indicates a cluster shape between an area-filling shape, where volume scales as  $(\text{length})^2$ , and a volume-filling shape (such as spheres) where volume scales as  $(\text{length})^3$ . Furthermore, the exponent corresponds to the fractal dimension of invasion percolation and indicates that the volume of clusters during fractional flow scales within percolation universality class. The length of the largest cluster is restricted by the length of the sample and/or field of view and, therefore, the largest clusters do not follow the general distribution. Once a cluster percolates from bottom to the top of our field of view, we can observe volume increase but cannot observe increase in length. This finite size effect is displayed as the maximum  $Ca^{\text{macro}}$  in all following figures.

### Pathway flow and Ganglion dynamics in the $S$ - $Ca$ -diagram

So far only individual clusters have been analyzed, while in the following we aim to characterize the complete flow regime involving all clusters. Therefore we consider average properties like saturation but also the averaged capillary number  $\overline{Ca}^{\text{macro}}$ , taking into account that each cluster has a different length and volume.

Trajectories based on the average  $\overline{Ca}^{\text{macro}}$  are shown in Figure 7. When ganglion dynamics occurs where the connected oil (grey) gets disconnected (yellow) and reconnected (Figure 7.1), the trajectory moves up and down in saturation and  $\overline{Ca}^{\text{macro}}$  (Figure 7.2). The reason for this is that when more clusters are disconnected, the saturation decreases, since the narrow pore throats connecting the oil phase are filled by water instead of oil. Moreover, the volume of the disconnected clusters and their

corresponding length becomes also smaller, which leads to a decrease in  $\overline{Ca}^{macro}$ . When the oil clusters become reconnected, the saturation and  $\overline{Ca}^{macro}$  increases again. Since  $\overline{Ca}^{macro}$  is limited due to the sample size, the trajectory is deflected at high saturations. On the other hand, the trajectory in connected pathway flow does not show any changes (Figure 7.4). Since the oil and water are moving through independent pathways, the cluster shape is not changing as shown in Figure 7.3.

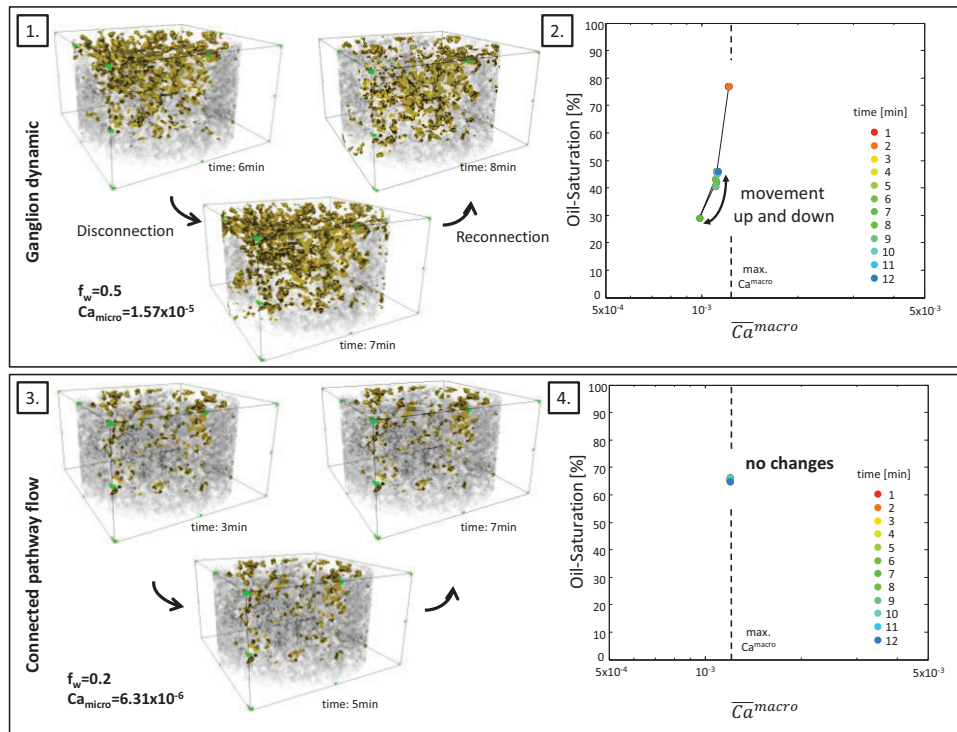


**Figure 7** It depends on  $f_w$  whether ganglion dynamics ( $f_w = 0.5$ ) or pathway flow ( $f_w = 0.2$ ) occurs. While at  $f_w = 0.5$  the oil gets disconnected (yellow) and reconnected (grey) during quasi steady-state conditions (1), the oil distribution remains constant at  $f_w = 0.2$ . The  $S-Ca_o^{macro}$  diagram shows that the clusters at  $f_w = 0.5$  move up and down the trajectory (2), while the clusters at  $f_w = 0.2$  remain at one point (4). However, in both cases  $\overline{Ca}^{macro}$  is close to the maximal possible  $Ca^{macro}$ , which is limited by the sample size.

### Contribution to the relative permeability

Since the ganglion dynamics observed on the  $S-\overline{Ca}^{macro}$  diagram correlates with the pressure and saturation fluctuations, all observations in core flood experiments appearing at the same water fraction ( $f_w = 0.5$ ) may be also associated with ganglion dynamics. However, at least at the pore scale, the impact on relative permeability is not as clear so far. In Figure 8, the development of the relative permeability through the continuous oil and water phase with time is shown, excluding the contribution of disconnected clusters via ganglion dynamics. Since the injection rate and water fraction  $f_w$  was constant over time, the deflection in relative permeability between the sixth and eighth minutes represents the contribution of ganglion dynamics.

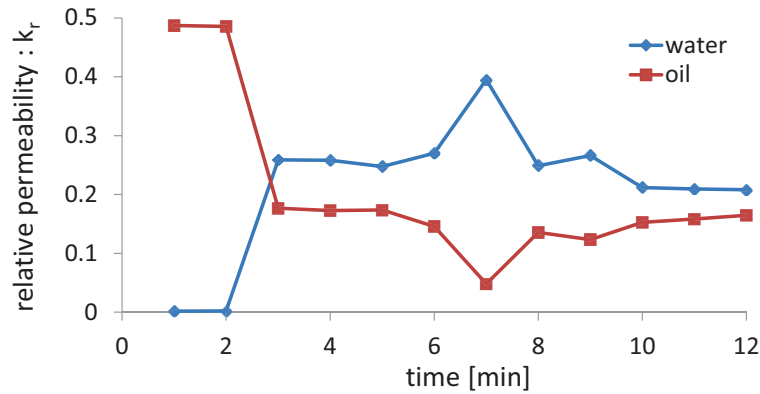


**Figure 8** Relative permeability at  $f_w = 0.5$  and high  $Ca$  during time. At this high flow rate, the quasi steady-state conditions are reached already after one minute. As the saturation (Figure 2) and the relative permeability of the oil and the water remains stable, a disconnection and reconnection (Figure 7) corresponding to a moving ganglion can be observed, whereby a disconnection causes an increase of the relative permeability of the water and a decrease for oil.

## CONCLUSIONS

Flow regimes during fractional flow have been characterized by imaging the pore-scale fluid distribution using synchrotron-based fast X-ray computed microtomography. We observed regimes of connected pathway flow but also ganglion dynamics regime. These flow regimes can be categorized in the fractional flow vs. capillary number ( $f_w$ - $Ca$ ) space. In order to construct a phase diagram indicating which flow regime prevails at which conditions, we sampled this space by conducting steady-state  $\mu$ CT flow experiments, which in addition to pressure and saturation data allows us to identify the respective flow regimes from the pore-scale displacements and oil cluster (ganglion) movement.

Oil clusters follow distinct trajectories in the saturation- $Ca$  space, which is caused by pore-scale displacement events. Pore-scale processes such as cluster coalescence and growing cause an increase in cluster volume and length so that the clusters move up a trajectory in a saturation and capillary number diagram. In break-up processes, both volume and length decreases and clusters move down the trajectory. Averaging over all clusters of a measurement for each time step allows us to characterize the flow regime involving all clusters in our field of view. Since almost no events occur at connected pathway flow, no changes can be observed at the saturation- $Ca$  diagram. On the other hand, ganglion dynamics cause a movement both up and down the trajectory.

These pore-scale processes clearly affect two-phase flow at larger scales. Fluctuations in saturation and pressure, as observed in Darcy-scale steady-state relative permeability experiments, have very similar characteristics to those observed in our  $\mu$ CT flow experiments. That clearly indicates that the pressure and saturation fluctuations observed on a 5 cm-long rock sample at intermediate fractional flow and saturation ranges are likely to be related to ganglion dynamics. The different flow regimes contribute differently to the total flow. Due to break-up and coalescence in a ganglion dynamics

flow regime, the connectivity is changing what affects the flow and causes change in relative permeability. This has to be considered for describing two-phase flow by numerical models.

## ACKNOWLEDGEMENTS

We would like to acknowledge Kevin Mader and Marco Stampanoni (Tomcat beamline at the Swiss Light Source of Paul Scherrer Institute, Villigen, Switzerland). We thank Alex Schwing and Rob Neiteler for the design of the flow set-up and instrumentation, Ab Coorn, Fons Marcelis and Niels Brussee for sample preparation, Hilbert van der Linde, Niels Brussee and Sebastiaan Pieterse for the steady-state relative permeability measurements, and Axel Makurat for helpful discussions and leadership support. We gratefully acknowledge Shell Global Solutions International B.V. for permission to publish this work.

## REFERENCES

1. Buckley, S. and Leverett, M., “Mechanism of fluid displacement in sands”, *Transactions of the AIME* (1942) 146.01, 107–116.
2. Berg, S., Cense, A. W., Hofman, J. P., Smits, R. M. M., “Two-Phase Flow in Porous Media with Slip Boundary Condition”, *Transp Porous Med.* (2007) 74:275–292.
3. Avraam, D. G. and Payatakes, A. C., “Flow regimes and relative permeabilities during steady-state two-phase flow in porous media”, *Journal of Fluid Mechanics* (1995) 293, 207–236.
4. Tsakiroglou, C. D., Aggelopoulos, C. A., Terzi, K., Avraam, D. G., Valavanides, M., “Explicit correlation of the steady-state-two phase relative permeability functions of porous media with the local flow rate”, SCA2014-041.
5. Datta, S. S., Dupin, J. B. and Weitz, D. A., “Fluid breakup during simultaneous two-phase flow through a three-dimensional porous medium”. *Physics of Fluids* (2014) 26(6), 062004.
6. Raeini, A. Q., Blunt, M. J., Bijeljic, B., “Direct simulations of two-phase flow on micro-CT images of porous media and upscaling of pore-scale forces”, *Advances in Water Resources* (2014) 74, 116-126.
7. Lopez, O., Mock, A., Skretting, J., Petersen, E.B.Jr, Øren, P.E., Rustad, A.B., “Investigation into the reliability of predictive pore-scale modeling for siliciclastic reservoir rocks”, SCA2010-41.
8. Valavanides, M. S. (2014), “Operational efficiency map and flow characterization for steady state two-phase flow in porous media”, SCA2014-047.
9. Armstrong, R. T. and Berg, S., “Interfacial velocities and capillary pressure gradients during Haines jumps”, *Physical Review E* (2013) 88(4).
10. Youssef, S., Bauer, D., Bekri, S., Rosenberg, E., Vizika, O. “3D In-Situ Fluid Distribution Imaging at the Pore Scale as a New Tool for Multiphase Flow Studies”, *SPE* (2010) 135194.

11. Georgiadis, A., Berg, S., Makurat, A., Maitland, G., Ott, H., “Pore-scale micro-computed-tomography imaging: Nonwetting-phase cluster-size distribution during drainage and imbibition”, *Physical Review E* (2013), 88, 033002.
12. Youssef, S., Bauer, D., Peysson, Y., Vizika, O., “Investigation of Pore Structure Impact on the Mobilization of Trapped Oil by Surfactant Injection”, SCA2014-064.
13. X. Pak, T., Butler, I.B., Geiger, S., Van Dijke, M.I.J. and Sorbie, K.S., “Droplet fragmentation: 3D imaging of a previously unidentified pore-scale process during multiphase flow in porous media.” (2015), *Proceedings of the National Academy of Sciences*, 112(7), 1947-1952.
14. Haines, W. B., “Studies in the physical properties of soil. V. The hysteresis effect in capillary properties, and the modes of moisture distribution associated therewith”, *The Journal of Agricultural Science*, (1930) 20(97), 97–116.
15. Berg, S., Ott, H., Klapp, S. A., Schwing, A., Neiteler, R., Brussee, N., Makurat, A., Leu, L, Enzmann, F., Schwarz, J.-O., Wolf, M., Kersten, M., Irvine, S., Stampanoni, M., “Real-time 3D imaging of Haines jumps in porous media flow”, *Proceedings of the National Academy of Sciences*, (2013) 110(10), 3755–3759.
16. Berg, S., Armstrong, R. T., Georgiadis, A., Klapp, S. A., Schwing, A. Neiteler, R., Brussee, N., Makurat, A., Leu, L, Enzmann, F., Schwarz, J.-O., Wolf, M., Khan, F., Kersten, M., Irvine, S., Stampanoni, M., “Multiphase flow in porous rock imaged under dynamic flow conditions with fast x-ray computed microtomography”, SCA2013-011.
17. Youssef, S., Rosenberg, E., Deschamps, H., Oughanem, R., Maire, E., Mokso, R., “Oil ganglia dynamics in natural porous media during surfactant flooding captured by ultra-fast x-ray microtomography”, SCA2014-023.
18. Berg, S., Armstrong, R. T., Georgiadis, A., Ott, H., Schwing, A. Neiteler, R., Brussee, N., Makurat, A., Rücker, M., Leu, Wolf, M., Khan, F., Enzmann, F., Kersten, M., “Onset of oil mobilization and non-wetting phase cluster size distribution”, SCA2014-026.
19. Roof, J. G., “Snap-off of oil droplets in water-wet pores”, *SPEJ* (1970) 10(1), 85–90.
20. Armstrong, R. T., Ott, H., Georgiadis, A., Rücker, M., Schwing, A., Berg, S., “Subsecond pore-scale displacement processes and relaxation dynamics in multiphase flow”, *Water Resources Research* (2014) 50, 9162–9176.
21. Tuller, M. and Or, D., “Hydraulic conductivity of variably saturated porous media: Film and corner flow in angular pore space”, *Water Resources Research*, (2001) 37(5), 1257–1276.
22. Morrow, N., “Physics and thermodynamics of capillary action in porous media”, *Ind. Eng. Chem.* (1970) 62(6), 32–56.
23. Wildenschild, D.; Culligan, K. A.; Christensen, B. S. B., “Application of x-ray microtomography to environmental fluid flow problems”, In U. Bonse (Ed.), *Developments in X-Ray Tomography IV Proceedings of SPIE* (2004) 5535, pp. 432–441.
24. Armstrong R. T., Georgiadis, A., Ott, H., Klemin, D., Berg, S., “Desaturation studied with fast X-ray computed microtomography”, *Geophysical Research Letters* (2014), 41, 55–60.